Published by:
Research Signpost
37/661(2), Fort P.O., Trivandrum-695 023, Kerala, India

Recent Res. Devel. Mat. Sci., 4(2003): 1-24 ISBN: 81-271-0022-6

Melt grown composite ceramics obtained by directional solidification: structural and functional applications.

Rosa I. Merino, José I. Peña, Ángel Larrea, Germán F. de la Fuente and Victor M. Orera
Instituto de Ciencia de Materiales de Aragón, C.S.I.C.- Universidad de Zaragoza, Pedro Cerbuna 12, E-50009 Zaragoza, Spain

Abstract

Eutectics grown from the melt are a paradigm of micron scale composite materials with improved properties. The improved mechanical properties and thermal stability, as compared to conventional polycrystalline ceramics, are consequences of the huge amounts of interfaces present in eutectics. Interface morphology and ordered structures invite to explore also other properties for regular eutectics of wide band gap materials, such as light guiding effects, anisotropic ion conduction, etc. The paper describes the properties of directionally solidified eutectic (DSE) oxides and fluorides, for example Al_2O_3-stabilized ZrO_2, NiO-stabilized ZrO_2 or CaF_2-MgO. The crystallographic and/or microstructural characteristics of selected systems will be compiled, as a function of growth conditions. It will be shown to which extent microstructure can be controlled for intended applications: optimum mechanical performance at high

Correspondence/Reprint request: Dr. Rosa I. Merino, Instituto de Ciencia de Materiales de Aragón, C.S.I.C.- Universidad de Zaragoza, Pedro Cerbuna 12, E-50009 Zaragoza, Spain. E-mail: rmerino@unizar.es

temperatures, mastering optical properties (light guiding, luminescence), generating porous crystalline materials or the existence of anisotropic ionic conduction.

Introduction

In situ composites obtained by solidification of eutectics have been studied for decades, mostly metal-metal composites, because of their superior mechanical properties. It is in this area where most advances in the comprehension of the eutectic growth characteristics and eutectic microstructures have been performed [1]. Fewer efforts were devoted to the area of ceramic eutectics except for those pioneering on oxide-oxide eutectics, as Al_2O_3-ZrO_2 or ZrO_2-$CaZrO_3$ [2]. The extraordinary mechanical response and excellent thermal stability promoted thorough studies of the microstructure and crystallography of several directionally solidified oxide eutectics [3]. The interest in those subjects has not decreased with time, and with the ever better microstructural characterisation techniques, the X-ray structural orientation relationships between the phases forming the directionally solidified eutectic was accurately determined. This characterisation was complemented by careful transmission electron microscopy observations [4]. X-ray diffraction techniques have also allowed the precise determination of residual stresses existent in the in-situ composite mostly as a consequence of the different thermal expansion characteristics of the component phases and the epitaxial relationship [5]. Residual stresses can strongly influence the mechanical properties of the composite materials.

In a different direction of research, nearly four decades ago, Galasso [6] drew attention to the potentialities that directionally solidified eutectics could have for applications different than structural ones, namely optical, electronic or magnetic, summarising in his paper the systems that had been grown in a controlled way throughout the world. Nevertheless, this direction of research does not seem to have deserved a strong attention of the specialists in the field to date.

During the last decade some new studies devoted to directional solidification of in-situ eutectic ceramic composites have been published [7, 8]. Renewed interest is mainly due to the high strength fibres obtained; strength which is also retained up to high temperatures. It is during these latter years when we have undertaken in our laboratory the task of producing directionally solidified ceramic eutectics, intended both for structural applications as well as for the investigation of optical and electrical properties. In this report we will summarise the main achievements obtained at the same time that we describe some new perspectives for this line of research.

Growth procedures

Eutectics grown from the melt give rise to highly structured dense materials The fine microstructure leads to composites with high density of interfacial area, strongly bonded interfaces and microstructural and chemical stability up to temperatures approaching the eutectic temperature. If the growth conditions are appropriate, interphase spacing can be kept under control by the growth rate and very homogeneous microstructrures with controlled grain size can be attained [9]. Moreover, when directionally grown, their microstructures can be aligned macroscopically. In that case their physical properties can also be macroscopically anisotropic. The key to attain all these features during growth is to keep micro- and macroscopically flat solid-liquid interfaces during growth, thus preventing constitutional undercooling and minimising convection in the melt. To grow ceramic eutectics, several

growth procedures are available [10,4]. Here we will describe the ones we used to grow oxide-oxide as well as fluoride-fluoride and oxide-fluoride eutectics. In tables 1 and 2 we give data corresponding to these eutectics which we have grown and of the individual single phases respectively.

a. Oxide-oxide eutectics

These kind of eutectics have high melting temperatures (above 1800ºC) and can be usually grown in air atmospheres by the laser floating zone method (LFZ). We used CO_2 laser heating to produce small molten volumes into a laser floating zone chamber, described elsewhere.[11] Feed rods were prepared from eutectic mixtures of commercial powders of the

Table 1. Composition and physical properties of the eutectic mixtures described in this work.

Compounds	Melting point (K)	Composition (%wt)	%vol. minor phase	Observed microstructure*
LiF-CaF_2	1055	0.46 CaF_2 + 0.54 LiF	41.6 CaF_2	L
NaF-$NaMgF_3$	1105	0.293 MgF_2 + 0.707 NaF	44 $NaMgF_3$	DL evolving to NaF F
CaF_2-MgO	1625	0.9 CaF_2 + 0.1 MgO	10 MgO	F
ZrO_2-Al_2O_3	2135	0.42 ZrO_2 + 0.58 Al_2O_3	33 ZrO_2	DL, F in col. or L in cells
Al_2O_3-$Y_3Al_5O_{12}$	2100	0.335 Y_2O_3 + 0.665 Al_2O_3	45 Al_2O_3	DL faceted
$CaZrO_3$-ZrO_2(CaO)	2525	0.56 $CaZrO_3$ + 0.44 $Ca_{0.25}Zr_{0.75}O_{1.75}$	41 CaSZ	L
MgO-ZrO_2	2445	0.21 MgO + 0.79 $Mg_{0.2}Zr_{0.8}O_{1.8}$	28 MgO	F
NiO-CaSZ[#] (or YSZ[&])	2115	0.61 NiO +0.39 $Ca_{0.15}Zr_{0.85}O_{1.85}$	44 CaSZ	L
CoO-CaSZ[#] (or YSZ[&])	2025	0.64 CoO + 0.36 $Ca_{0.11}Zr_{0.89}O_{1.89}$	38.5CaSZ	L
ZrO_2(Y_2O_3)-$NiAl_2O_4$	2270	0.54 $NiAl_2O_4$ +0.46 $Zr_{0.85}Y_{0.15}O_{1.92}$	39 YSZ	F of YSZ in col.

* L: lamellae, F: fibrous, DL: degenerate lamellae, F in col.: fibres in colonies

[#] YSZ = Yttria stabilised zirconia

[&] CaSZ = Calcia stabilised zirconia

Table 2. Physical properties of the individual components of the above listed eutectic mixtures and related compounds.

Compound	density (g/cc)	Melting Point T_m (K)	Melting entropy $\Delta H_m/RT_m$ [(a)] [12]	Thermal expansion α x 10^6 K^{-1}	n (550 nm) [13]
LiF	2.657 [13]	1121 [12]	2.91	34.4 [13]	1.39
CaF_2	3.181 [13]	1691 [12]	2.11	18.9 [13]	1.44
NaF	2.164 [13]	1269 [12]	3.16	33.5 [13]	1.34
$NaMgF_3$	3.091 [14]	1303	6.09 [15]		
MgO	3.583 [13]	3105 [12]	3.01	13 [16]	1.75
ZrO_2	5.6 [17]	2950 [12]	3.55	7.5	2.19
Al_2O_3	3.987 [13]	2327 [12]	5.74	8.2 [18]	1.76
YAG	4.554 [13]	2210 [19]		8.9 [20]	1.84
$CaZrO_3$	4.82 [14]	2823			2.15
$Ca_{0.2}Zr_{0.8}O_{1.8}$	5.37 [14]			12.9	2.2
NiO	6.69[17]	2228 [12]	2.94	16.5 [20]	2.18 [17]
CoO	6.45 [17]	2078 [12]	3.15		
$NiAl_2O_4$	4.50 [21]	2373 [22]		8.41 [23]	
$Y_{0.16}Zr_{0.84}O_{1.92}$	5.94 [13]	3110 [13]		10.6 [18]	2.18
$MgAl_2O_4$	3.577 [13]	2408 [12]	9.82	8.8 [24]	1.72

[(a)] R = 8.31441 J K^{-1} mol^{-1}

components, conformed as rods around 3 mm diameter by isostatic pressing. They obtained sufficient handling strength by pressureless sintering at temperatures around 1500 ºC. Growth rate could be varied between 10 and 1500 mm/h. The main characteristics of this growth procedure are: 1) no crucible or die is used, and thus contamination with foreign impurities which could perturb the solidification process is minimised. 2) The melt volume is small, only several mm^3, allowing on the one side the melting of high melting point materials with moderate laser powers, and minimising on the other side convection in the melt, which might otherwise perturb liquid-solid interphase flatness. And 3) steep temperature gradients are built at the solid-liquid interphase. This allows the use of fast growing rates without constitutional undercooling, and thus maintaining coupled growth conditions. Unfortunatelly this high axial temperature gradient is associated to a high radial temperature gradient that can cause cracking of the growing rod or the accumulation of radial thermal stresses which will cause cracking of the sample during subsequent manipulation. This was observed by Peña et al. [25] in the growth of $ZrO_2(Y_2O_3)$-Al_2O_3 eutectics, and prevented by the use of small diameter bars (less than 2 mm). In this case the gradient at the solidification interface was determined to be $6x10^5$ K/m. In general, the gradient at the interphase is dependent on the growth equipment (focusing system, growth rate) as well as on the thermal diffusion to the external atmosphere

and along the rod (influenced by thermal conductivity and rod diameter). High speed rotation of the growing bar homogenises the melt and works in favour of a macroscopically more planar solid-liquid interface, and would allow larger diameter bars free of cracks. Nevertheless, liquid viscosity and misalignments on the LFZ apparatus may difficult the use of rotation for small diameter samples.

The bar shaped samples, although very useful for mechanical testing or physical characterisation in general (measurement of residual stresses, ionic or electronic conduction, light guiding effects, etc.), present a limitation in relation to some possible applications requiring large surfaces. This has prompted us to use laser surface melting as a technique to produce flat plates of directionally solidified eutectics [26]. In this case the laser beam is conveniently shaped as a thin, long-line (typically 1mmx10mm) by using mirrors or lenses, and make to hit the surface of the ceramic precursor. The thin long line has the advantage over a single spot (as used by Bourban et al.[27]) that the surface processed in one single run is larger and edge effects diminished. In this case the solidification front is not planar from a macroscopic point of view. The longitudinal section of the melt-crystal front is sketched in figure 1. The local solidification direction changes with the vertical position of the volume element being melted, to keep it perpendicular to the solid-liquid interphase. Maybe more important than this when analysing the resultant microstructure is the fact that local growth rate is also dependent on vertical position, and as a consequence interphase spacing (λ) has to change to adapt to the local solidifidation rate (V), following the $\lambda^2 V$ = Constant rule [28].

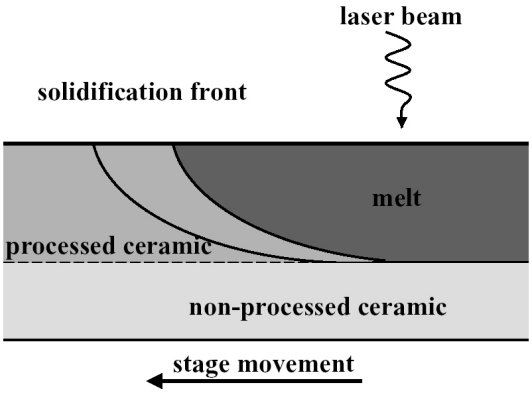

Figure 1. Schematics showing the shape of the solidification front in laser processed plates.

b. Fluoride containing eutectics

A number of fluoride-fluoride eutectics have been grown in the past [29], although they have not been thoroughly studied. These eutectics have a low melting temperature and have to be grown in oxygen free, water free atmospheres. We have used the Bridgman method to grow the CaF_2-LiF, CaF_2-MgO and NaF-$NaMgF_3$ eutectics with the composition given in table 1. We used a radio-frequency heated furnace using vitreous carbon crucibles in Ar inert atmosphere at a rate of 5 mm/h. No precursor ceramics were needed. The final samples were cylinders 1.7 cm^2 x 10 cm size, and the eutectic grain size reached several cubic millimetres.

Microstructure

Besides the lower melting temperature of the eutectics when compared with their constituent phases, the eutectic solids present a very fine microstructure with clean interfaces. The relevant properties of the melt processed eutectics stem from their microstructural features. It is particularly important to know to which degree the microstructure can be considered to be homogeneous, as it occurs in coupled growth, or whether it consists mainly of colonies separated by intercolony regions. Equally relevant is the determination of the size and internal morphology of the eutectic grains and the relative orientation of the fibres or lamellae between adjacent grains, the faceted or non-faceted nature of the interfaces, the degree of alignment in the case of directionally solidified eutectics, the interphase spacing that can be achieved within a particular microstructure, etc. When the growth is within the coupled regime one can properly speak of eutectic grains [28]. Directional solidification imposes a preferential orientation for the grains. Their size along and across the solidification direction is governed by the growth equipment and conditions and the ability of the growing material to accomodate to fluctuations. The range of applications of eutectic systems depends on the physical properties of the component phases as much as on the above listed microstructural features of the solidified eutectic. Therefore, in this section we will discuss on the microstructure of the eutectics referred to in table 1.

A first guess of the expected microstructure can be obtained from the data given in table 1. Assuming isotropic oxide-oxide interphases, the criteria of minimum interfacial energy for a given eutectic mixture that follows coupled growth implies that lamellae are formed if the volume of the minor phase is above 28% and hexagonal rod lattice arrangement when it is lower. In table 1, last column, we have included information of the actual microstructure observed. Most of the eutectic systems follow the phase volume rule. Alternating lamellae or fibres embedded in a matrix of the other phase form the basic building structure of these eutectics.

Three of the systems appear to violate the general phase volume rule above mentioned in different ways. In the case of NaF-$NaMgF_3$ transverse and longitudinal cross-sections of the microstructure are shown in figure 2. Degenerate lamellae are observed all over the sample, which mainly organise inside faceted grains (see figure 2 a). A longitudinal cross-section of well ordered areas is presented in figure 2.b. It is this alignment that makes the sample transmit light efficiently along the growth direction. An observation with higher magnification of the ordered regions (fig. 2 c) shows a strong tendency of the lamellae to arrange following a hexagonal fibrous pattern of the major NaF phase. That is to say, the cross-section aspect ratio of the NaF lamellae is small and they are bent to cover a hypothetical hexagonal lattice.

The eutectics $NiAl_2O_4$-YSZ produced in our laboratory between 30 and 200 mm/h and ZrO_2-Al_2O_3 produced at not so low growing rates, by our group [25] as well as by other authors, present the complex-regular microstructures shown in figure 3. It consists of highly ordered colonies with zirconia fibres in a hexagonal arrangement inside the $NiAl_2O_4$ or Al_2O_3 matrix. In the latter case it arises because of the high fusion entropy characteristic of Al_2O_3. According to the Hunt and Jackson criterion [1], isotropic growth with no facets of a eutectic mixture is possible when both phases have low entropy of melting, $\Delta S/R<2$. If this is the case, crystals are neither expected to grow faceted, nor to have an extremely fast growth rate. Both characteristics favour the coupled growth of the component phases. At very low growth rates (10 mm/h) we observed coupled growth in Al_2O_3-ZrO_2 eutectics, with a characteristic interpenetrating microstructure. When growth rate increases, the homogeneous degenerate lamellae microstructure evolves to colonies, which eventually becomes faceted for growth

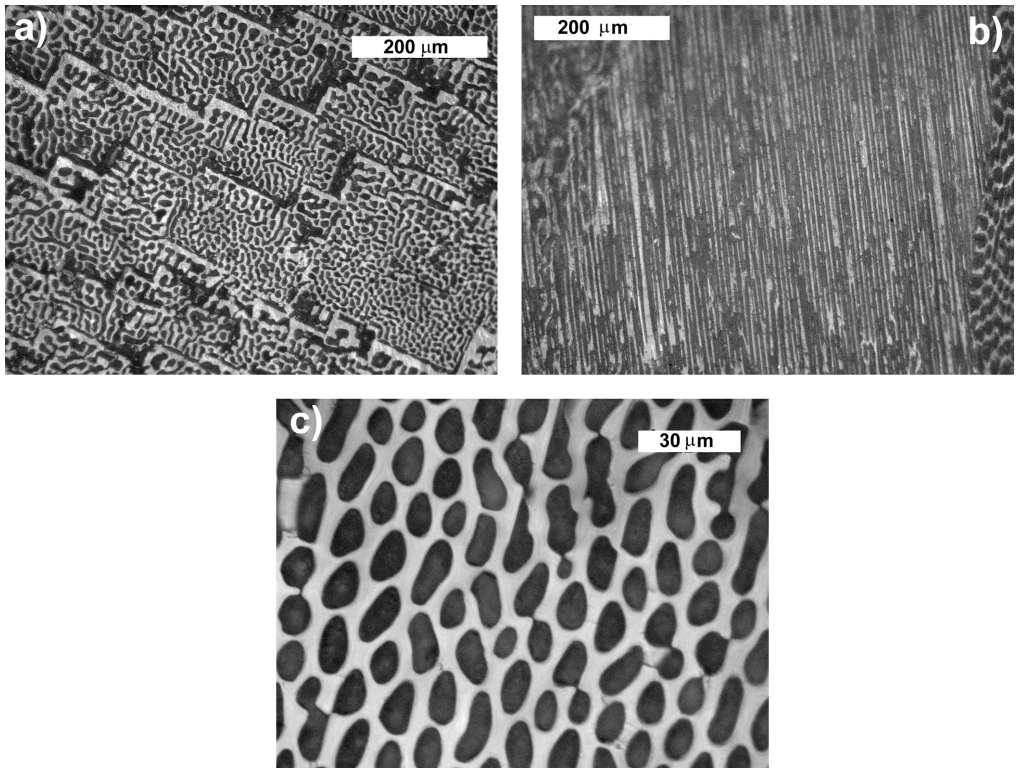

Figure 2. Optical micrographs of a transverse (a and c) and longitudinal (b) cross-section of the melt grown NaF-$NaMgF_3$ grown at 5 mm/h. The surface has been etched to appreciate better the microstructure. Bright: $NaMgF_3$, dark: holes corresponding to disolved NaF phase.

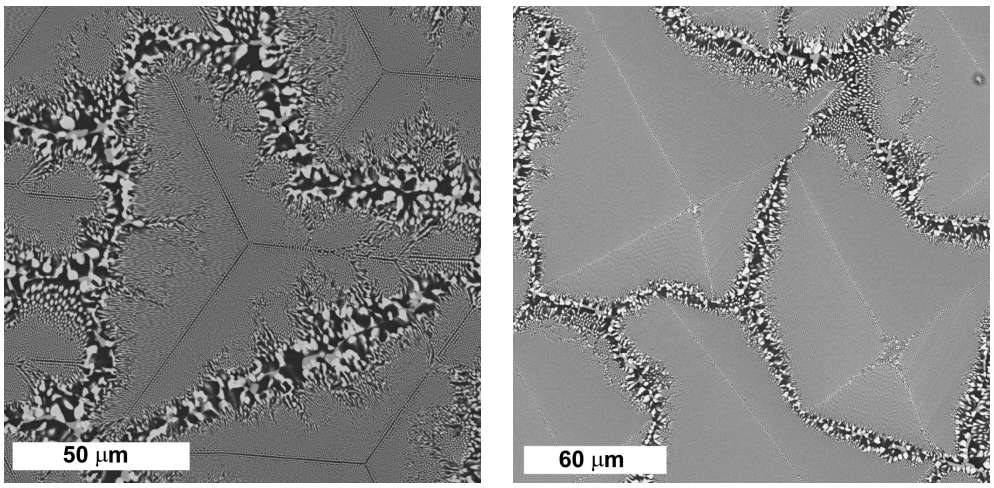

Figure. 3. Transverse cross sections of the eutectics Al_2O_3-YSZ (left) and $NiAl_2O_4$-YSZ (right) showing colonies.

rates above 100 mm/h approximately. In this regime all published crystallographic analyses coincide in the conclusion that the Al_2O_3 phase grows parallel to the c direction [30, 25, 31]. Faceting of these Al_2O_3 growing crystals in R-plane facets cause ZrO_2 fibres to align perpendicular to those facets, along [110] cubic zirconia directions. This combination gives rise to the observed microstructure. Consequently, it is the increased supercooling produced at these growth rates that induces faster growth speed of the more stable Al_2O_3 crystalline phase (see table 2), which leads the growth of the eutectic.

The eutectic $NiAl_2O_4$-YSZ composition is determined here for the first time. Its composition and melting temperature is given the table 1. While the theoretical volume fraction of the minor phase is near 39%, its dominant microstructure is fibrous. In figure 4 we observe the long, parallel YSZ fibres arranged inside colonies. The volume fraction of YSZ measured by image analysis of cross-section images inside the colonies (highly ordered regions) ranges between 32 and 38 %, which is in accord with the theoretical value. Although we have not jet performed the study of the evolution of the microstructure with the growth rates for the YSZ-$NiAl_2O_4$ eutectic, which could give us a complete picture of the factors controlling the microstructure, the analogy with the much better known Al_2O_3-ZrO_2 system is giving us some clues. The observed colonies have here a square rather than a triangular shape, which must also be associated with faceting of the matrix $NiAl_2O_4$ grains. We have not found in the literature information on the entropy of melting for this compound. As a model compound showing the same crystal structure we give $MgAl_2O_4$ in table 2. It shows a very high entropy of melting. As expected, $NiAl_2O_4$ will present similar values, so that it is not surprising to find such a complex-regular, faceted colony microstructure for the eutectic. In fact, Kennard et al. [32] observed that $MgAl_2O_4$-MgO eutectics grown at speeds faster than 20 mm/h also show faceted colony growth with shapes similar to what we observe in $NiAl_2O_4$-YSZ. It is to be noted that single crystals of $NiAl_2O_4$ grown by the floating zone method grow along <100> direction showing four facets [33]. This seems to be the phase leading the

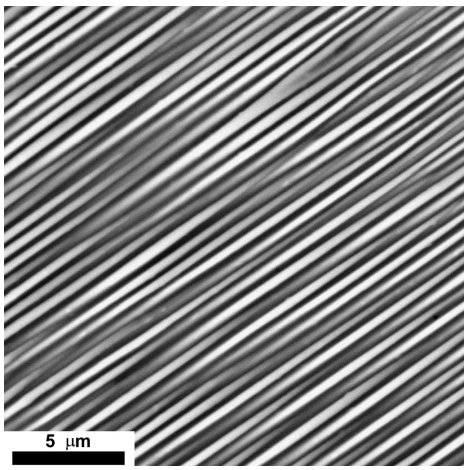

Figure 4. Scanning Electron Microscopy (SEM) micrograph of the eutectic YSZ-$NiAl_2O_4$ showing the perfect alignment of YSZ fibres (bright in the image) inside the colonies.

growth, originating also the discrepancy between the volume fraction prediction and the true microstructure.

The composition of this eutectic was determined by electron probe micro analysis of eutectic like microstructures in solidified samples with varying composition, from $ZrO_2(Y_2O_3)$-Al_2O_3 to $ZrO_2(Y_2O_3)$-NiO. For the identification of the crystallographic phases we used micro raman dispersion spectra (see figure 5). The spectra in the fibrous region (a) is dominated by the highly raman active tetragonal zirconia, showing its characteristic peaks. In the darkest phase (spectra (b) and (c)), apart from leaking light which comes from the surrounding zirconia phase, new features between 300 and 400 cm^{-1} are clearly observed. They correspond to the maxima around 320 cm^{-1} and 370 cm^{-1} associated with $NiAl_2O_4$, as shown in spectrum (d).

The other anomalous eutectic is the Al_2O_3-YAG directionally solidified eutectic. Its microstructure has been observed to be of the homogeneous Chinese Script type in fibres grown by the μ-pulling down method at speeds from 90 mm/h to 600 mm/h by Epelbaum [34]. This microstructure is a kind of degenerate lamellae arrangement, which builds up an interpenetrating bicrystal. It presents almost planar sharp interfaces between phases that bent at sharp angles instead of showing curved smooth interphases, more common in interpenetrating ZrO_2-Al_2O_3. When processed by surface remelting of a flat ceramic pellet with the equipment described above, the microstructure turns to cellular, as it can be observed in figure 6. The sharply faceted inter-phase interfaces between Al_2O_3 and YAG can nevertheless be clearly distinguished. In figure 7 we compare details in both systems grown at

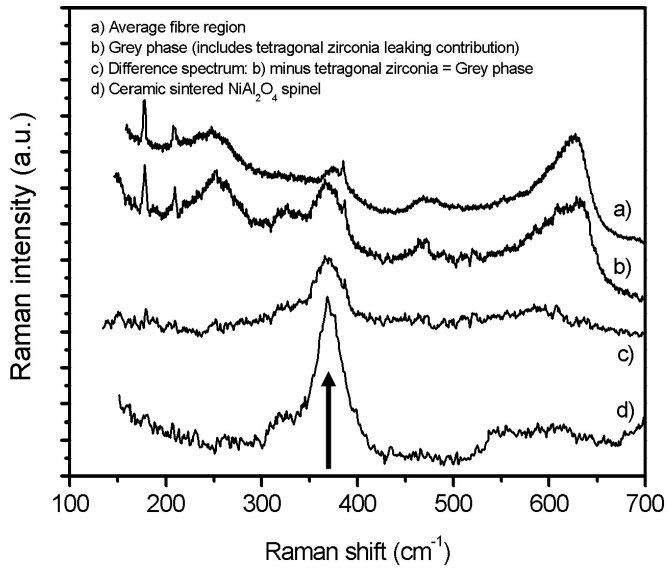

Figure 5. Raman spectra [35] of different phases in grown $NiAl_2O_4$-YSZ eutectic. The spectrum measured in $NiAl_2O_4$ produced by solid state reaction is also shown for comparison. The arrow indicates the position at about 370 cm^{-1} characteristic of $NiAl_2O_4$ which is also present in the eutectic mixture spectra (b).

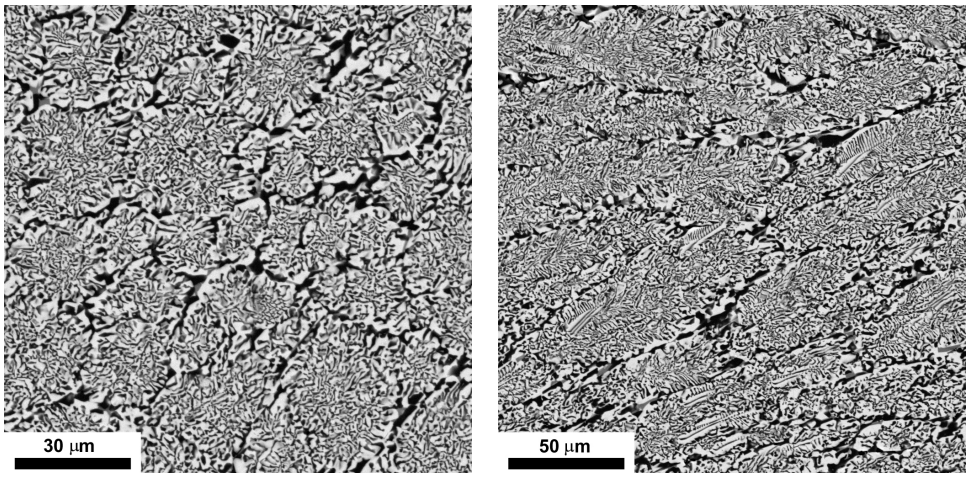

Figure 6. Transverse (left) and longitudinal (right) cross-section of the eutectic Al_2O_3-YAG plate. Processing speed 500 mm/h.

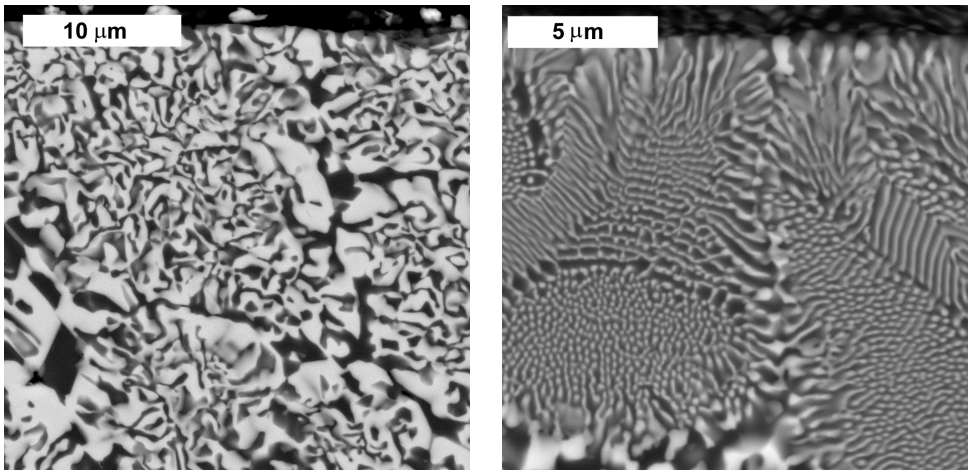

Figure 7. SEM transverse cross-section micrographs near the surface of Al_2O_3-YAG (left) and Al_2O3-$ZrO_2(Y_2O_3)$ (right) samples grown at 500mm/h. Note the jagged inter-phase interfaces in the first case.

500 mm/h. The formation of cells is probably associated to the change in solidification direction with distance to the external surface, whereas the apparently jagged interphases between Al_2O_3 and YAG could be associated with a large crystallographic anisotropy.

The rest of compositions present the expected microstructure. CaSZ-NiO, CaSZ-CoO and CaSZ-$CaZrO_3$ show beautiful lamellar arrangements, which indeed are capable to adapt to

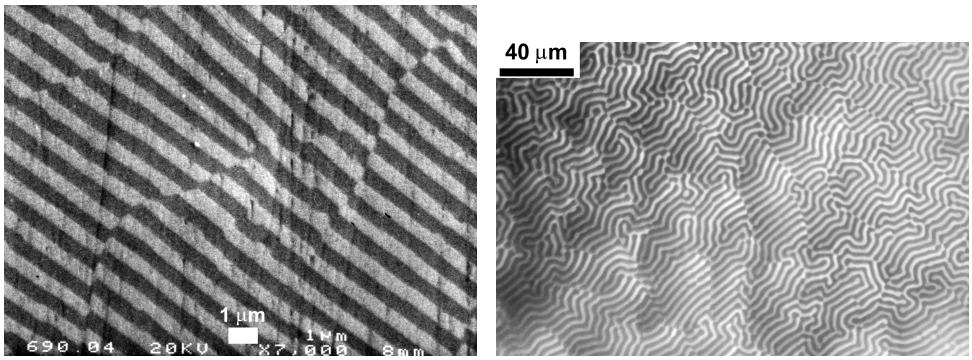

Figure 8 Details of transverse cross sections of ZrO_2(CaO)-NiO (left) and ZrO_2(CaO)-$CaZrO_3$ (right) eutectics. The brighter corresponds to stabilized zirconia in both cases.

variations of the solidification rate. In figure 8 we give transverse cross-sections of selected areas of these samples. In view of the micrographs, the latter system shows less faceted phase1-phase2 interphases than the previous ones. This can be related with the absence of an exact orientation relationship pattern. In fact, for LFZ grown CaSZ-$CaZrO_3$ samples, whereas average approximate orientation relationships can be given from X-ray diffraction pole figures [36], ($(100)_{CSZ}$ approx. // $(011)_{pseudocubic\ CaZrO3}$ and $(010)_{CSZ}$ approx. // $(100)_{pseudocubic\ CaZrO3}$) precise TEM diffraction experiments [37] show that there is no exact epitaxial relationships between both component phases. This lack of epitaxial relationship and the fact that interfaces are not faceted is probably the reason why one can obtain large (several mm^3 size regions by LFZ) regions of well aligned lamellae arrangements, and thus think on applications of such a kind of microstructure. In the eutectic compositions $Co_{1-x}Ni_xO$-ZrO_2, even for large variations in the growth direction, the interphase plane orientation relationship $\{111\}Co_{1-x}Ni_xO//\{100\}ZrO_2$ has been found for all compositions [38]. Once more, recourse to the Hunt and Jackson criterion can be made. There is no data available for the entropy of melting of $CaZrO_3$, and a value of 3.55 for non-doped zirconia was found. The doped one will be somewhat lower, thus approaching the limit value of 2 which could allow coupled growth and confer the ability of adaptation to small variations of solidification rate or composition during growth. Since neither NiO nor CoO entropy values deviate very much from 2, this will be also nearly applicable to its eutectic with stabilized zirconia. We have also grown NiO-CaSZ eutectic plates at higher growth rates (3600 mm/h). In that case, eutectic grains tended to transform to cells that meet each other without inter-cell phases.

The fluorides LiF, CaF_2 and NaF have a comparatively low entropy of melting. Consequently, a similar behaviour is observed in the eutectics in which they take part, which have regular or nearly regular microstructures. See for example figure 9 for an optical micrograph of LiF-CaF_2. Also shown in that figure is an optical micrograph of the CaF_2-MgO eutectic. The 10%vol MgO phase arranges as fibres embedded into the CaF_2. The interphases are semifaceted, with an exact epitaxial relationship between both phases which built two planar, low-energy interphases ($\{100\}_{CaF2}$ // $\{111\}_{MgO}$) and two curved ones [39]. Grain sizes are typically of 400 μm in size. The higher $\Delta S/R$ value of $NaMgF_3$ makes the microstructure of the eutectic $NaMgF_3$-NaF irregular, with clearly faceted $NaMgF_3$ grains, as explained above.

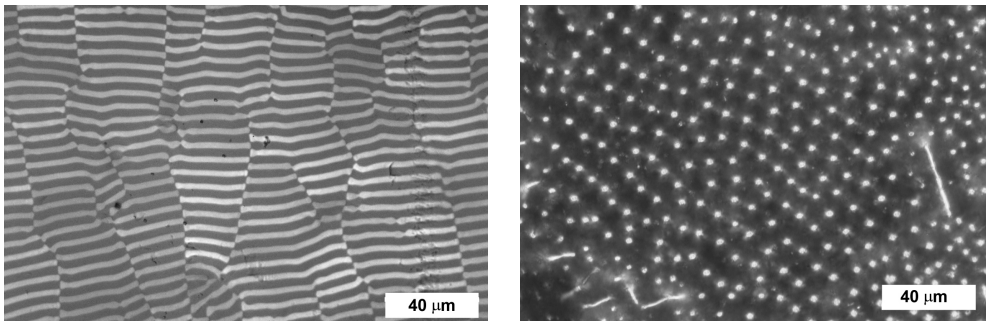

Figure 9. Transmission optical micrograph of the eutectics LiF-CaF_2 (left) and CaF_2-MgO (right). The brighter phase correspond to CaF_2 and MgO respectively (phase with the larger refractive index in each couple).

The interphase spacing as a function of growth rate for all the samples studied are compiled in figure 10. These are reported for regular microstructures as well as for complex-regular ones, the latter measured in the ordered areas inside the colonies. In many eutectic systems the law $\lambda^2 V$ = constant has been observed [3], which is expected from the hypothesis of growth at the extremum in regular eutectics. The lines depicted in the figure follow that law

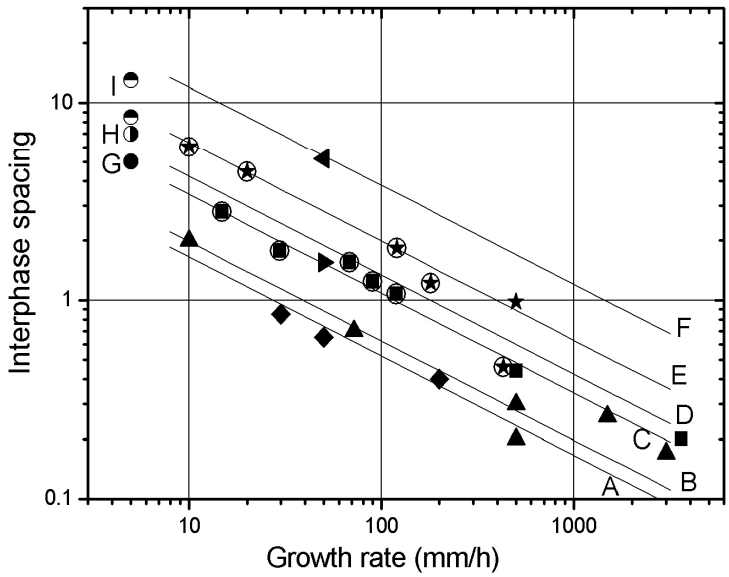

Figure 10. Interphase spacing as a function of growth rate for some eutectic systems. Symbols make reference to experimental points extracted from our experiments, except for those enclosed in a circle, which have been extracted from the references indicated in table 3. Each family has been fitted to the $\lambda^2 V$ =constant law (straight lines). Whenever only one point was available, the data to display the line were taken from the literature. Refer to table 3 for full details.

with the constant given in table 3. For the eutectics grown by the Bridgman technique only one solidification rate is available. In the rest of the samples the most systematic study has been made for the ZrO_2-Al_2O_3 system, which nevertheless shows some data dispersion because it goes through different regimes of growth across the full growth rate range. The explored range in YSZ-$NiAl_2O_4$ fits l the rule satisfactorily, as well as the YSZ-NiO system, where the low rate data have been taken from the literature [40] The measured interphase spacing inside the Al_2O_3-YAG colonies grown at 500 mm/h fits well with the extrapolation of lower growth rate data of Epelbaum [34]. We can observe that in all cases interphase spacing ranges between 0.1 to 10 μm, with regular microstructures in the neighbourhood of 1 μm for oxides and 5 to 10 μm for fluorides. This is important at the moment of designing materials for intended uses, where one definite microstructure, quality of ordering and size of the microstructural features combination is required. Some properties will be revised below. Of course, the range of coupled growth is dependent to some extent on the crystal growth equipment, but solidification gradients have a limit if crack free samples are needed or when heat extraction from the solidifying front is limited by the intrinsic thermal conductivity of the growing crystal.

Table 3. Values of C in the law $\lambda^2 V=C$ for the systems plotted in figure 10.

Index, symbol (Figure 10)	Eutectic System	C (μm^2 mm/h)	Reference (This work +)
A, ◆	$ZrO_2(Y_2O_3)$-$NiAl_2O_4$	27.4	
B, ▲	$ZrO_2(Y_2O_3)$-Al_2O_3	39	
C, ■, ●	NiO-CaSZ	117	[40]
D, ▶	MgO-ZrO_2	180	[3]
E, ★, ✪	Al_2O_3-$Y_3Al_5O_{12}$	395	[34]
F, ◀	$CaZrO_3$-ZrO_2(CaO)	1450	[3]
G , ●	LiF-CaF_2	122	
H, ◑	CaF_2-MgO	245	
I, ◓	NaF-$NaMgF_3$	552	

Melt grown composites as structural materials. Residual stresses

As it was pointed above, the interest of directional solidification of ceramic eutectics arises mainly from their higher strength and fracture toughness when compared with that of the corresponding single phase materials, together with good retention of mechanical properties in oxidising environments at high temperatures. Examples of this behaviour are Al_2O_3-YAG [41, 42, 43] and YSZ-Al_2O_3 [44, 45] directionally solidified eutectics. Even ductile behaviour at high temperatures with high strength has been observed in Al_2O_3-$GdAlO_3$ DSE [46].

The room temperature tensile strength is dependent on the actual microstructural features. Up to date the most extensively studied system is Al_2O_3-YSZ DSE. Its strength depends on the Y_2O_3 content and microstructure. Best performance has been reported for samples with either tetragonal or cubic zirconia and crack free fine rods. Values of 1.1 GPa [45], 1.5 GPa [47] or 2 GPa [48] have been reported for samples grown under different conditions. Together with high flexural strength, this material also presents high fracture toughness values of 7.8 MPa $m^{1/2}$ [45]. Besides having very clean interfaces, residual stresses

also contribute to crack bridging and overlapping, which are effective toughening mechanisms in brittle solids. It appears that the limiting size defect for colony microstructures is the size of the colony, which as explained above can be prevented to form at sufficiently slow growth rates. Fracture tests, performed on rods of 1.5 mm diameter with the interpenetrating microstructure, have given reproducible tensile strengths over 1.5 GPa [49]. In this regime the microstructure (interlamellar spacing as well as aspect ratio of the lamellae) does not change with the amount of Y_2O_3 used to form solid solution with the ZrO_2 [50]. This is shown in figure 11 for the range of compositions investigated. The zirconia phase however goes from monoclinic, in the Y_2O_3 free sample, through tetragonal to cubic YSZ upon increasing Y_2O_3 content. At the same time, the residual stresses present in the composite vary from one composition to the other. This is caused by the mismatch of thermal expansion between ZrO_2 and Al_2O_3 from the solidification temperature to RT and by the ZrO_2 martensitic transformation. Residual stresses which have a strong influence on the mechanical properties were studied by Pardo [51], Harlan [50] and Orera [52] as a function of microstructure [51], Y_2O_3 content [50] and also at low temperatures [52].

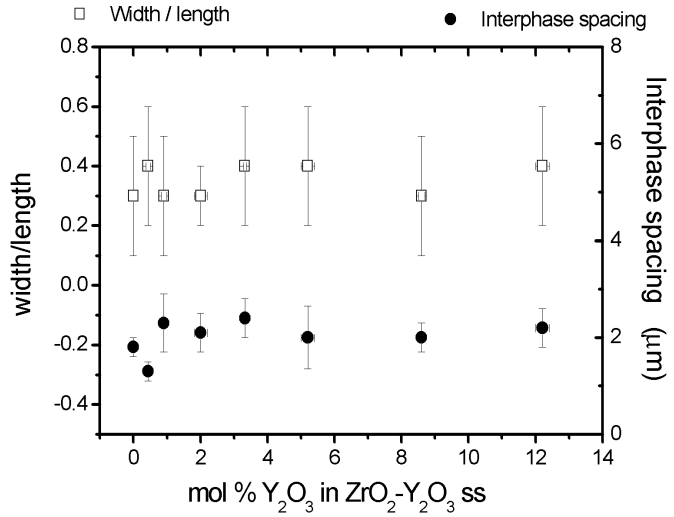

Figure 11. Microstructural features (width/length of ZrO2 lamellae and interphase spacing) versus Y_2O_3 content in YSZ-Al_2O_3 DSE.

Among the techniques available for this purpose, the piezospectroscopic methods are easy to use, do not require complicated preparation of the samples and calibration exists for a considerable number of materials [53]. Particularly the Cr^{3+} traces present in commercial Al_2O_3 are enough to give an intense R-lines luminescence, whose wavelengths are very sensitive to the stress state of the hosting Al_2O_3 [54]. The stresses turn out to be strongly anisotropic in the samples with Y_2O_3 content below 1%, where more than half of the zirconia is in its monoclinic phase. The hydrostatic component is tensile in Al_2O_3 at low Y content, goes through zero at about 1.5% Y_2O_3 and becomes compressive above it. The anisotropy in the stress state is not surprising given the highly textured and aligned microstructure of DSE. Comparison with calculations based on a self-consistent model indicates that the stresses are the expected ones for strongly bonded interphases between ZrO_2 and Al_2O_3 and indicate that

stress relaxation mechanisms exist in monoclinic zirconia eutectics with monoclinic zirconia. The main source of stress relaxation is in this case microcracking. This microcracking of the Al_2O_3 phase is more profuse in the DSE with the largest interphase spacing, being inhibited in the finely microstructured ones [55]. In any case the mechanical properties of eutectics containing monoclinic zirconia are not expected to be good because the Al_2O_3 phase is under tensile stress.

More information can be extracted from low temperature piezospectroscopic measurements since it increases the resolution. Orera et al. [52] have shown that the width of the distribution of the residual stresses can be obtained directly from the ruby luminescence spectrum taken at 77K. In table 4 we give values of the average hydrostatic stress (σ_h) and the width of the distribution for the Al_2O_3-ZrO_2 composite with different Y contents. As expected for thermoelastic stresses, stresses decrease in magnitude in t-ZrO_2 - Al_2O_3 and c-ZrO_2 –Al_2O_3 DSE on increasing temperature. Release of thermal stresses at high temperatures (T > 1000C) produces a decrease in the mechanical properties of the material.

Table 4. Residual stress value at 77K and its FWHM (MPa) in Al_2O_3-ZrO_2 DSE with interpenetrating microstructure for different Y_2O_3 content.

Sample type	σ_h (MPa)	$\Delta\sigma_h$ (MPa)
m-ZrO_2-Al_2O_3	540±15	950
t-ZrO_2 - Al_2O_3	-510±10	420
c-ZrO_2 –Al_2O_3	-460±10	520

Residual stresses have also been determined in other DSE by X-ray diffraction techniques. YAG and Al_2O_3 have similar thermal expansion coefficient and no phase transition from the melting temperature to RT, so that their eutectic is not expected to have high residual stress values, as has been measured by Dickey [5]. On the contrary high residual stresses develop in NiO-YSZ DSE [56] corresponding to the large difference in thermal expansion coefficient. It appears that also in this system the interphases are strongly bonded and must correspond to low energy interfaces [57].

Eutectics as photonic materials: Doping with optically active ions

Except for the eutectics containing transition metal ion oxides, the compounds listed in table 1 are transparent in the visible and near infrared range, and therefore suitable for optical applications. The relatively large (several mm side) ordered regions that can be fabricated with CaSZ-$CaZrO_3$, LiF-CaF_2 lamellar arrangement, as well as CaF_2-MgO fibrous ordering allows one to think of them as single crystalline stacks of planar waveguides or optical fibres respectively. Refractive index contrast (see data in table 1), and guiding phase thickness or diameter are appropriate for single mode guiding in the visible or near infrared range. A clear example of this behaviour is illustrated by the transmission optical micrographs presented in figures 8b and 9, where the bright phases are the ones along which light is guided in the visible range. A deeper detailed analysis has been performed in Er^{3+} doped CaSZ-$CaZrO_3$ eutectic by Orera et al. [58]. They also demonstrated [59] the fabrication of active planar waveguides in these wide gap material, injecting IR laser light into single CaSZ lamellae and measuring on the other end the up-conversion Er^{3+} luminescence at 0.545 μm. There is to be noted that single mode propagation can take place at 500 nm (green light) into the fibrous ordered

regions of Al_2O_3-ZrO_2 eutectics. Trials to get macroscopic size ordered regions of this eutectic are underway. This seems to be possible once a quite complete picture of the relationships between growth conditions, microstructure and crystallographic relationships between Al_2O_3 and ZrO_2 has been gained, as explained in the previous paragraphs.

The transparent phase eutectics have to be doped with optically active ions in order to make them optically active, and to induce for example fotoluminescence or cathodoluminesncence. As with single crystals, doping has been performed by adding small amounts of the corresponding oxide or fluoride to the starting materials, which are subsequently melted and solidified. The result of doping CaSZ-$CaZrO_3$ with Er^{3+} is that both component phases get Er^{3+}, with 3 times more Er in the highly defective CaSZ matrix than in $CaZrO_3$ perovskite [60]. Also, quantum efficiency is larger in CaZrO3:Er^{3+} than in CaSZ:Er^{3+}, where larger multiphonon relaxation probability is observed. As a consequence, luminescence can emerge from the eutectic sample through either of the component phases depending on the excitation or detection range, and the synergy of combining two materials with different optical behaviours is an advantage over single phase materials. Note also that, even if one is not interested into the ordered microstructure of DSE, from the optical point of view it is better in general to have a fully dense material, with clean interphases free of pores, rather than a compacted and sintered ceramic, where impurities or residual porosity might reside at grain boundaries increasing light scattering.

The micron scale microstructure of dielectric ordered structures has also important effects into the luminescence of defects or active impurities. A practical example are the photonic crystals where certain luminescence wavelengths can be either completely inhibited or forced to radiate only at definite directions of the photonic crystal structure. Ordered fibre eutectics are microstructures suitable for 2D photonic crystal applications, but up to now no such effects have been reported. A much less impressive effect, but also related to the modification of the available electromagnetic modes to radiate due to the presence at very short distances (of the order of the wavelength) of a different dielectric medium has been observed in Er^{3+} doped Al_2O_3-ZrO_2 eutectics. Al_2O_3 is a bad host for Er^{3+}, and actually it can be introduced in the sapphire matrix only by low temperature procedures. In the Al_2O_3-ZrO_2 eutectic grown from the melt this ion enters exclusively the ZrO_2 matrix in either of the microstructures achieved. The $^4I_{13/2}$ level luminescences around 1.5 μm, which is comparable to the width of the ZrO_2 phase into the eutectic. Consequently its luminescence probability becomes modified by the nearby presence of the lower refractive index Al_2O_3 phase. In figure 12 we show how the lifetime and the size of the YSZ phase are correlated in the right direction: lifetime increases (and radiative transition probability decreases) going to thinner lamellae of the high refractive index media inside the lower refractive index matrix [61]. Note that the residual stresses in YSZ, as measured by piezospectroscopy in Al_2O_3, are not the origin of the change in lifetime since there is no correlation between both magnitudes.

Another application, which we would like to report on, is the possibility of using the DSE LiF-CaF_2 as a dosimeter. We doped the eutectic with MnF_2. A difference with CaF_2 single crystals is its greater resistance to cleavage. The material is translucent and isotropic from the optical point of view. Also, being a dense material it resists surface attack better than ceramics producing a very efficient thermoluminescent material that combines two

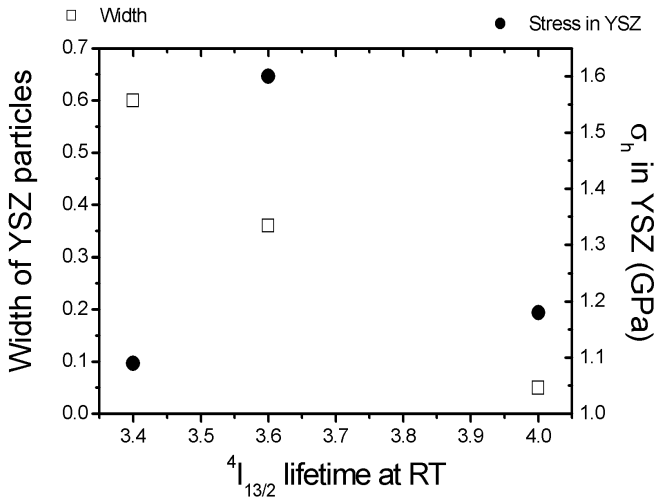

Figure 12. Correlation between lifetime of Er^{3+} $^4I_{13/2}$ level with the width of the YSZ particles in the DSE. The value of the hydrostatic component of stress in YSZ is also shown.

complementary dosimeters, for low and high doses. A detailed analysis of its dosimeter characteristics will be given elsewhere [62].

Use of DSE in optical devices may be hampered by the relatively small size of the eutectic grains, but they can be competitive with other tailored materials in the sub-millimetre size range.

Ionic conductivity in stabilized zirconia containing eutectics

Another important area of application where DSE may have its slot is electroceramics. One first approach can be made taking advantage of the good mechanical properties of some eutectics as compared to single crystal phases (see for example stabilized zirconia). This could allow thinner electrolyte films to be manufactured without loss of their mechanical performance. The price one has to pay is a decreased volume fraction of the ionic conducting phase in the case of YSZ-Al_2O_3, CaSZ-$CaZrO_3$ or MgSZ-MgO eutectics. As an added value, directional solidification confers to the material anisotropic conduction properties. This has been observed in these three materials [63, 64, 65]. Of course conductivity is larger along the growth direction in composites with conducting fibre inclusions.

In an attempt to benefit from the excellent mechanical strength, bar shaped samples with lengths up to 100 mm, and appropriate ionic conduction of YSZ-Al_2O_3 were produced. We tested it as a Nernst glower element. The maximum temperature of use should be lower than the eutectic point. Microstructural evolution was observed to be low up to 1500ºC [25], at least for interpenetrating microstructures. The average thermal expansion of the composite along the growth direction is $8.3x10^{-6}$ K^{-1} from RT to 900ºC, less than pure YSZ, moreover they withstand relatively fast heating and cooling cycles being dense. A DSE with composition $ZrO_2(5.6\%Y_2O_3)$-Al_2O_3, hot zone of 7 mm, around 1.2 mm diameter and preheated to 815ºC reached 1600 ºC upon dissipating 14 watt Joule heat. We kept the sample in these conditions for about 160h, to evaluate the changes in conductivity as well as in microstructure induced by

these working conditions. In figure 13 we show the conductivity of the sample, before and after the test, together with values measured at high temperatures. Neither mechanical damage or conductivity deterioration was observed on the sample after the test. The Arrhenius dependence with temperature is the one expected for YSZ, showing lower activation energy at high temperatures (around 0.8 eV) and near to 1 eV below 600 ºC (see Figure 13).

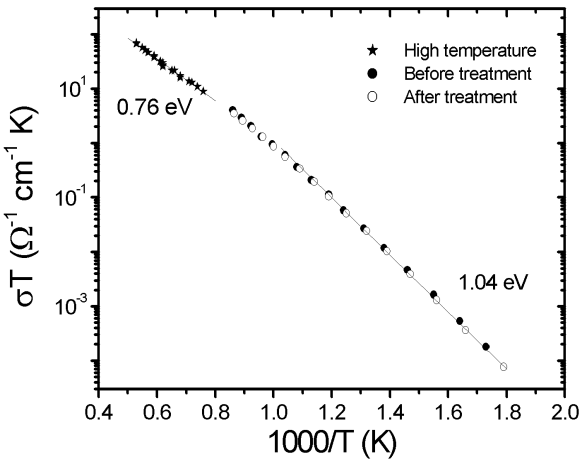

Figure 13. Ionic conductivity of as grown and thermally treated $ZrO_2(Y_2O_3)$-Al_2O_3 DSE´s.

The microstructure, on the contrary, has suffered severe changes. Before treatment the sample showed the degenerate-colony microstructure shown in figure 14 a. After treatment, the transverse SEM micrographs show an external corona with small increase of the particle size, whereas the core of the cylinder showed large ZrO_2 particles into the Al_2O_3 matrix (see figure 14). It is not easy to know the internal temperature of the rod during treatment, but in any case it is high enough to cause strong coarsening of the microstructure. This coarsening has not affected the structural integrity of the sample but we do not know yet whether or to what extent the mechanical properties have been affected.

One appealing second approach to enter relevant to the electroceramics field is the possibility that DSE offer to control interphase spacing in composite material at the same time that one can have confidence in having got clean, possibly low energy interfaces. It has been observed in some composites produced by different methods with a finely dispersed second phase, or in nanocrystalline materials, that ionic conductivity can be enhanced by several orders of magnitude. Although there is still controversy whether the reason for that behaviour is space charge distribution [66], strain fields at the interfaces [67], or some other reason depending on the actual material and preparation conditions, it seems clear that the conductivity of nanocrystalline grain boundary regions is greater than that in bulk crystals. Even in zirconia solid solutions this effect has been observed. A similar effect in DSE has not been observed up to date. One reason must be the limited range of interphase spacings that could be explored. In figure 10 we can observe that typical interphase spacings are in the

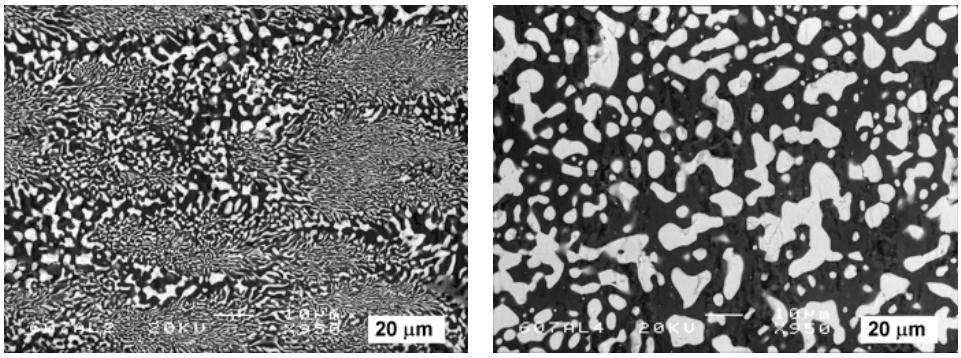

Figure 14. Longitudinal cross-sections of $ZrO_2(Y_2O_3)$-Al_2O_3 DSE before (left) and after (right) treatment. Central region of the rod. The micrographs are enlarged by the same amount for ease of comparison.

micron range, far enough form the tenths of nm thickness required to observe any enhancement in YSZ electrolytes. We obtained minimum interphase spacings of 200 nm in YSZ-Al_2O_3 DSE, forming cells with lamellae arrangement inside. The thichness of YSZ in these samples lies around 80 nm, problably not enough to see any effect in this good electrolyte. It is probably worthwhile to look for appropriate eutectics where the relevant conducting phase shows more probability of interface enhancement of conductivity at this thickness range. The benefits of achieving a better conducting electrolyte with thermally and mechanically stable microstructure, as is the case with DSE, are worth the effort.

Cermets from controlled reduction of eutectics

One area where those ionic conducting materials would be readily applied would be in the Solid Oxide Fuel Cell research and development. Microstructural stability and good thermomechanical response are relevant aspects of concern. This is particularly true with respect to anodes. The state of the art anode for Solid Oxide Fuel Cells is the porous Ni-YSZ cermet. Here a YSZ skeleton houses the Ni percolating particles, and is intended to prevent severe clustering in order to achieve large triple phase boundary lengths (extension of the length over which pores, Ni particles and YSZ phase meet). Since DSE present a very homogeneous, fine microstructure, and the eutectic composition of NiO-YSZ possesses a convenient volume fraction of components, it can be used as a precursor to produce Ni-YSZ porous cermets. Such an approach has been followed, and preliminary results of YSZ films deposited on Ni-YSZ anodes produced by laser assisted directional solidification of plates have been reported elsewhere [68, 69]. The microstructure of these cermets consists of a YSZ skeleton, organised as lamellae eutectic grains, separated by porous Ni lamellae. The transformation of the as-grown NiO-YSZ eutectic to Ni-YSZ cermet upon reduction treatments is controlled by oxygen diffusion. Oxygen is transported out from the ceramic composite along the oxide ion conducting YSZ and the compensating electron transport proceeds through Ni particles. The result is a material with 43% vol YSZ + 33.5 % Ni + 23.5% pores, in which electrical conductivity along the growth direction is electronic, controlled by the Ni phase. Note that conductivity, chemical diffusion [70], as well as the magnetic properties of the cermet derived from the ferromagnetic metallic particles are expected to be

anisotropic. Moreover, the triple phase boundary length can be modified with the growth conditions. In figure 10 the intephase spacing of the eutectic can be found between 2 and 0.2 μm, which means a factor of about 10 in phase boundary length.

A second example of cermet derived form thermochemical reduction of eutectics is shown in figure 15. It corresponds to the reduction of the eutectic $NiAl_2O_4$-YSZ. At high temperatures in H_2 rich atmospheres $NiAl_2O_4$ spinel transforms to its equilibrium phase Ni+α-Al_2O_3 (if there is no kinetic hindering), whereas YSZ remains unchanged. It is nevertheless important that YSZ is present in the eutectic since it provides paths for $O^{=}$ transport, which makes possible a more homogeneous reduction all over the sample. Reduction at 900ºC in 7%H_2-N_2 (for 6 hours) produces partial reduction of the $NiAl_2O_4$ matrix phase showing submicrometric bright particles in the SEM micrographs (fig 15 a and b). They correspond probably to Ni particles inside a porous Ni deficient spinel matrix. Reduction at 1300 ºC generates also pores and cracks in the spinel phase (see figure 15 c and d), and the observed Ni particles are disperse, and consequently do not give rise to any electronic conductivity. Detailed observations [71] show that the Ni particles nucleate on the surface of YSZ fibres (intracolony) or on YSZ intercolony particles, and grow from these nuclei. This reveals the importance of having a homogeneous distribution of YSZ across the sample to provide homogeneous distribution of nucleating points and easy paths to deliver oxygen to the outside of the sample. Nevertheless, still inhomogeneities in the Ni particle distribution are observed. Once nucleated, the growth (or coalescence) of the particles takes place in the neighbourhood of the intercolony areas. This is particularly visible in the inner part of the rods (2 mm

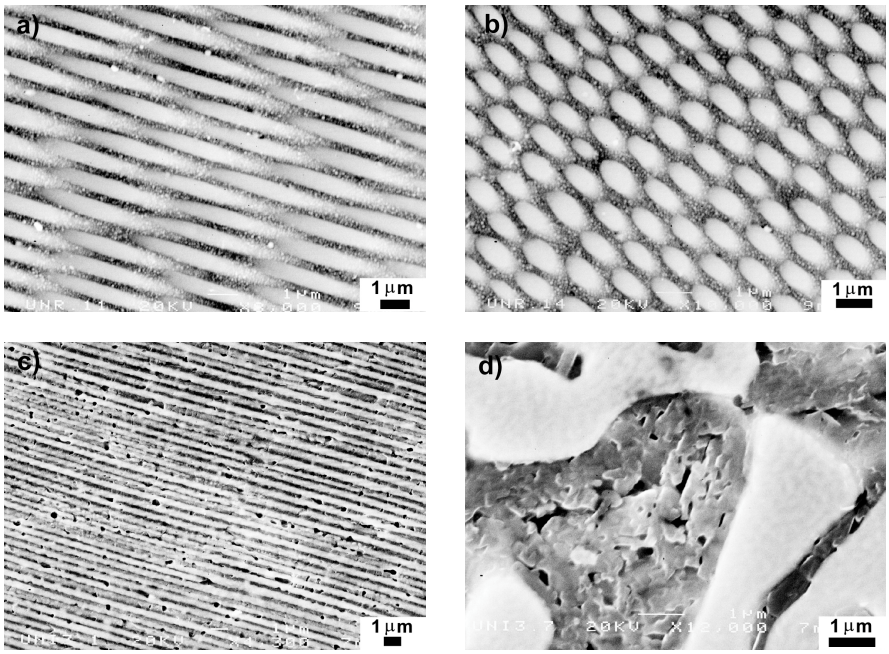

Figure 15. Details of a section of the eutectic $NiAl_2O_4$-YSZ after thermochemical treatments. a) and b) reduced at 900ºC, c) and d) at 1300 ºC. The observed surface has been polished before the treatments, therefore only occasionally we came across Ni particles in the sample reduced at 1300ºC.

diameter), revealing a slow oxygen diffusion process, which competes with cation diffusion in $NiAl_2O_4$.

Porous single crystals

The cermets we have just described contain a porosity volume below 25%. It can be even larger if one of the phases in one DSE is dissolved, while the other remains intact. For example, Ni or Co can be eliminated from Ni-YSZ or Co-YSZ cermets in weak acids. The result is a very fragile, around 50% volume pore YSZ formed by crystalline lamellae held together by the eutectic grain to grain contacts. Pore volumes as high as 55% could be achieved starting with $NaMgF_3$-NaF eutectics. NaF can be very easily disolved in water. The important characteristic in this latter case is $NaMgF_3$ that forms the matrix, occupies 45% of the volume, and has mechanical integrity such that it withstands subsequent manipulation.

Apart from being able to fabricate porous structures that can afterwards be infiltrated with desired compounds and thus translate the DS eutectic structure to virtually any combination of materials, either ceramic-ceramic, metal-ceramic, ceramic-organic, etc., we can in this way synthesise compositions which are not easy from single crystal growth techniques. Think for example on Ni of Co doped YSZ. Phase equilibria diagrams require that the incorporation of a solute to a solid-solution by melt processing starting from a particular melt solution composition is determined by the partition coefficient which depends on the breadth and slopes of the solidus and liquidus curves. On the other side, eutectic solidification requires simultaneous solidification of two compositions, each saturated with the other one, and thus the expected amount of solute into a particular compound reach its maximum possible value.

Conclusion

In the present work we have revised the results of ongoing research in the directional solidification of oxide and fluoride eutectics. The microstructural characteristics of the grown materials using laser float zone melting, laser surface remelting and Bridgmann growth techniques have been analysed. The most complete study has been made in the system $ZrO_2(Y_2O_3)$-Al_2O_3, where the biggest range of solidification rates (and solidification regimes) has been spanned. In all cases the $\lambda^2 V$=constant relationship between interphase spacing and solidification rate is obeyed. Practical solidification rates, originating crack free samples and homogeneous microstructures lay in the range form 0.1 to 10 μm. Some new eutectic compositions have also been determined and produced, namely $NiAl_2O_4$-YSZ and $NaMgF_3$-NaF. Both these compounds present an unexpected microstructure in the sense that fibrous microstructure dominates the $NiAl_2O_4$-YSZ eutectic with near 40 %vol YSZ fibres, and low aspect ratio lamellae inside a 45 %vol $NaMgF_3$ matrix is observed in the second one.

Once produced, we have focussed our interest in mechanical, optical and conductive properties, including the production of porous cermets or highly porous matrices. The benefits we pretend with the use of eutectics are based on the synergy arising from the combination of the properties of the two component materials into a single one, and the mutual interdependence. The very fine homogeneous microstructure of some YSZ-Al_2O_3 composites have shown the best mechanical properties up to date, including sustained strength up to high temperatures. Simultaneous Er^{3+} doping of CaSZ-$CaZrO_3$ or selective doping in ZrO_2 inside Al_2O_3-ZrO_2 have given equally interesting results with respect to Er^{3+} luminescence or guiding properties. The particular distribution of YSZ into $NiAl_2O_4$ to provide $O^{=}$ paths as well as

nucleation sites for Ni when the material is subjected to low oxygen partial pressures allows the production of dispersed Ni particles of nanometric size. Finally, note that we have produced a 55 % porous $NaMgF_3$ crystal.

Results are far from being complete and the possibilities offered by this kind of materials are only limited by the researcher interests. But first of all an exhaustive study of the microstructure and growth conditions has to be made in order to evaluate the expected performance of the system. The data given in figure 10 and in some reviews [1,2,3,4,9,10,28] published before should serve as a good guide.

Acknowledgment

This work has been supported by the Spanish Ministry of Science and Technology under contracts number MAT2000-1495 and MAT2000-1533-C03-02. The help of C. Estepa in the design and construction of some experimental equipment is gratefully acknowledged.

References

[1] Hunt, J.D. and. Jackson K.A. 1966 Trans Metal. Soc. AIME 236, 843-852. *Binary eutectic solidification*.
[2] Hulse, C.O. and Batt, J.A. 1974, Final Tech. Rept. UARL-N910803-10, NTIS AD-781995/6GA. *Effect of Eutectic Microstructures on the Mechanical Properties of Ceramic Oxides.*
[3] Minford, W.J., Bradt, R.C. and Stubican, V.S. 1979, J. Amer. Ceram. Soc. 62, 154..
[4] Revcolevschi, A., Dhalenne, G. and Michel, D. 1988, Mat. Sci. Forum 29, 173-198.
[5] Dickey, E.C., Frazer, C.S., Watkins, R.R. and Hubbard, C.R. 1999 J. Europ. Ceram. Soc. 2503-2509
[6] Galasso, F.S. 1967, Journal of Metals 17-21.
[7] Mah, T., Parthasarathy, T.A. and Matson, L.E. 1990, Ceram. Eng. Sci. Proc. 11, 1617-1627.
[8] Sayir, A., Farmer, S.C. Dickerson, P. O. and Yun, A.M. 1993, Mat. Res. Soc. Symp. Proc. 365, 21.27.
[9] Hunt, J.D. and Lu, S.Z. 1994 *Handook of Crystal Growth*, vol 2, Hurle, D.T.J. Editor, Elsevier Science. Chapter 14 *Crystallisation of Eutectics, Monotectics and Peritectics*.
[10] Ashbrook, R.L. 1977, J. Am. Ceram. Soc. 60, 428-435.
[11] de la Fuente, G.F., Díez, J.C., Angurel, L.A., Peña, J.I., Sotelo, A. and Navarro, R. 1995, Adv. Mater. 7, 853-856.
[12] I. Barin, and G. Platzki, Thermochemical Data of Pure Substances, VCH Weinheim, 1995.
[13] Data at RT from Tropf W.J., Thomas, M.E. and Harris, T.J. 1995 in *Handbook of optics, devices, measurements and properties*. 2nd Edition, Vol II. Bass, M. Ed., Mc Graw-Hill, Inc.
[14] From lattice parameter data.
[15] K. Adamkovikova, P. Fellner, L. Kosa, I. Nevad, I. Proks, J. Strecko, Thermochimica Acta (1994) 242, 23-6.
[16] Paladino A.E. and Snider, C.R. 1970. Amer. Ceram. Soc. Bull. 49. 280-285.
[17] Handbook of Physics and Chemistry.
[18] Green, D.J. 1998, *An Introduction to the Mechanical Properties of Ceramics*, Cambridge, Cambridge University Press. Clarke, D.R, Suresh, S. and Ward, I.M. Editors.
[19] V.S.Stankus, P.V. Tyagel´ski. J. Crsytal Growth 167 (1996) 165.
[20] Touloukian, Y.S., 1967, Thermophysical Properties of High Temperature Solid Materials, vol. 4, Oxides and their solutions and mixtures, MacMillan, New York.
[21] Landölt Börnstein New Series, III/4B, 1970, vol. 4, 449.
[22] R. Subramanian et al. J. Crystal Growth 143 (1994) 311-316.
[23] Lieberthal, M., Kaplan, W.D. 2001 Mat.Sci. Eng. A302, 83-91.
[24] Nitani, N., Yamashita, T., Matsuda, T., Kobayashi, S.I. and Ohmishi, T. 1999, J. Nucl. Mat. 274, 15-22.

[25] Peña, J.I., Merino, R.I., Harlan, N.R., Larrea, A., de la Fuente, G.F. and Orera, V.M. 2002, J. Eur. Ceram. Soc. 22, 2595.
[26] Larrea, A., de la Fuente, G.F., Merino, R.I. and Orera, V.M. 2002, J. Eur. Ceram. Soc. 22, 191.
[27] Bourban, S., Karapatis, N., Hofmann, H. and Kurz, W. 1997 Acta Mater, 45, 5069.
[28] Hogan, L.M., Kraft, R.W. and Lemkey, F.D., 1971, Advances in Materials Research 5, 83- 215.
[29] Rogalsky, G.I., Vettegren, V.I., Peller, V.V. , Ryzhov, V.A. and Hartmann, E. 1987, J. Cryst. Growth 82, 162-167.
[30] Starostin,M.Y., Gnesin, B.A. and Yalovets, T.N. 1997, J. Cryst. Growth 171, 119.
[31] Sayir, A., Farmer, S.C, 2000 Acta mater. 48, 4691-4697.
[32] Kennard, F.L., Bradt, R.C, and Stubican, V.S. 1973, J. Am. Ceram. Soc. 56, 566-569.
[33] Subramanian, R., Higuchi, M. and Dieckman, R. 1994, J. Crystal Growth 143, 311-316.
[34] Epelbaum, B.M., Yoshikawa, K., Shimamura, K., Fuluda, T., Suzuki, K and Waku, Y. 1999, J. Crystal Growth 198, 471-475.
[35] The help of Dr. M.L. Sanjuán in performing and analysing some Raman experiments is gratefully acknowledged.
[36] Santiso, J., Laukhin, V., Doudkowsky, M., Garcia, G., Figueras, A., Angurel, L.A., Merino, R.I., Peña, J.I., Sanjuán, M.L. and Orera, V.M. 2000, Adv. Mater. 12, 116.
[37] Larrea, A., Orera, V.M., Peña, J.I. and Merino, R.I. 1999, J. Mater. Res. 14, 2588..
[38] L.N. Brewer, V.P. Dravid, G. Dhalenne and M. Velazquez. 2002, J. Mater. Res. 17, 760.
[39] Larrea, A., Contreras, L., Merino, R.I., Llorca, J. and Orera, V.M. 2000, J. Mater. Res. 15, 1314.
[40] Dhalenne, G. And Revcolevschi, A. 1984, J. Crystal Growth 69, 616-618. Revcolevschi
[41] Mah, R., Parthasarathy, T.A. and Matson, L.E. 1990, Ceram. Eng. Sci. Proc. 11, 1617-1627.
[42] Mah, T., Parthasarathy, T.A., Petry, M.D. and Matson, L.E. 1993, Ceram, Eng. Sci. Proc. 14, 662-638.
[43] Waku, Y., Ohtsubo, H., Nakagawa, N. And Kohtoku, Y. 1996, J. Mat. Sci. 31, 4663-4670.
[44] Sayir, A. and Farmer, S.C. 2000, Acta Mater 48, 4691-4697.
[45] Pastor, J.Y., Poza, P., Llorca, J., Peña, J.I., Merino, R.I. and Orera V.M. 2001 Mat. Sci. Eng. A 308, 241.
[46] Waku, Y., Nakagawa, N., Wakamonto, T., Ohtsubo, H., Shimizu, K. And Kohtoku, Y. 1997, Nature 389, 49-52.
[47] Bates, H.E. 1992, Ceram. Eng. Sci. Proc. 13, 190.
[48] Farmer, S.C., Sayir, A. and Dickerson, P.O. 1993, *In situ Composites Science and Technology*, TMS, Warrendale, PA, 167-182.
[49] Llorca, J. et al. To be published.
[50] Harlan, N.R., Merino, R.I., Peña, J.I., Larrea, A., Orera, V.M., González, C., Poza, P. and Llorca, J. 2002, J. Am. Ceram. Soc. 85, 2025.
[51] Pardo, J.A., Merino, R.I., Orera, V.M. and Peña, J.I. 2000, J. Am. Ceram. Soc. 83, 2745.
[52] Orera, V.M., Cemborain, R., Merino, R.I., Peña, J.I. and Larrea, A. 2002, Acta Mater. 50, 4677.
[53] Ciacchi, L.C., Gregori, G., Lughi, V., Rossi, A. and Sergo, A. 1999, Recent . Res. Devel. Appl. Spectroscopy 2, 243-272.
[54] He, J. and Clarke, D. 1995, J. Am. Ceram. Soc. 78, 1347-1353.
[55] Merino, R.I., Peña, J.I., Harlan, N.R., de la Fuente, G.F., Larrea, A., Pardo, J.A., Orera, V.M., Pastor, J.Y., Poza, P. and Llorca, J. 2002 Ceram. Eng. Sci. Procceedings 23, 663.
[56] Dickey, E.C., Dravid, V.P. and Hubbard, C.R., 1997, J. Am. Ceram. Soc 80, 1773.
[57] Dravid, V.P., Lyman, C.E., Notis, M.R. and Revcolevschi, A. 1990, Metall Trans. A. 21 A, 2309.
[58] Orera, V.M., Peña, J.I., Merino, R.I., Lázaro, J.A., Vallés, J.A. and Rebolledo, M.A. 1997, Appl. Phys. Lett. 71, 2746.
[59] Orera, V.M., Merino, R.I., Pardo, J.A., Larrea, A., de la Fuente, G., Contreras, L., Peña, J.I. 2000, Acta Phys. Slovaca 50, 549.
[60] Merino, R.I., Pardo, J.A., Peña, J.I, de la Fuente, G.F., Larrea, A. and Orera, V.M. 1997, Phys. Rev. B 56, 10907.
[61] Merino, R.I., Pardo, J.A., Peña, J.I. and Orera, V.M. 2002, Appl. Phys. Lett. 80, 589.
[62] Chouiyakh, A., Gimeno. F., Peña, J.I., Contreras, L. And Orera, V.M. (to be published)

[63] Merino, R.I., Orera, V.M., de la Fuente, G.F. and Peña, J.I. 1996, Proceedings of the ELECTROCERAMICS V, International Conference on Electronic Ceramics and Applications, Aveiro, Portugal. Book 2, 131.
[64] Merino, R.I., Peña, J.I., Orera, V.M. and de la Fuente, G.F. 1997, Solid State Ionics 100, 313.
[65] Čička, R., Trnovcová, V. and Starostin, M. Yu. 2002, Solid State Ion. 148, 425-429.
[66] N. Sata, K. Eberman, K. Eberl and J. Maier. 2000, Nature, 408, 946- 949.
[67] D. Lubben and F.A. Modine, 1996, J. Appl. Phys. 80, 5150-5157.
[68] Merino, R.I., Peña, J.I., Laguna-Bercero, M.A., Larrea, A., and Orera, V.M. 2003, J. Eur. Ceram. Soc. (in press.)
[69] J.I. Peña, M.A. Laguna-Bercero, R.I. Merino, A. Larrea, V.M. Orera, G. García and A. Figueras, 2003, Ceramic Science and Engineering Proceedings (in press.)
[70] B. Bonvalot-Dubois, G. Dhalenne, J. Berthon, A. Revcolevschi and R.A. Rapp. 1988 J. Am. Ceram. Soc. 71, 296-301.
[71] C. Casas, Proyecto fin de carrera Report, University of Zaragoza, 2002.